Available online at www.ijournalse.org

Emerging Science Journal

(ISSN: 2610-9182)

Vol. 10, No. 3, June, 2026

Scenario-Robust Hydropower Suitability Mapping in Geothermal Regions Using Multi-Paradigm Spatial Modeling

Ahmad Saikhu [1*], Ira Mutiara Anjasmara [2], Widya Utama [2], Rista Fitri Indriani [2]

[1] *Department of Informatics, Institut Teknologi Sepuluh Nopember, Surabaya 60117, Indonesia.*

[2] *Department of Geomatics Engineering, Institut Teknologi Sepuluh Nopember, Surabaya 60117, Indonesia.*

Abstract

Hydropower planning in geothermal and environmentally sensitive regions involves substantial uncertainty due to complex terrain, ecological constraints, and competing land-use priorities. This study aims to evaluate whether the suitability patterns of hydropower that are robust to planning assumptions can be identified through cross-method spatial consistency rather than single-model optimization. We propose a scenario-based spatial decision-support framework that integrates knowledge-driven multi-criteria decision analysis (MCDA), supervised machine learning (XGBoost), unsupervised RLKM, and patch-based convolutional neural networks (PCNN) using harmonized satellite-derived spatial datasets. Three alternative planning scenarios, balanced, conservation-oriented, and energy-priority, are implemented through consistent feature-weighting schemes applied across all analytical paradigms. The evaluation focuses on internal robustness indicators, including cross-method agreement, scenario sensitivity, and spatial coherence, rather than external field validation. The results show that supervised learning models exhibit high performance stability across scenarios, whereas PCNN substantially improves spatial coherence by reducing the fragmentation of suitable zones. The MCDA provides a transparent and spatially contiguous baseline, whereas the RLKM reveals scenario-sensitive intrinsic suitability regimes. Areas consistently identified as suitable across methods and scenarios represent high-confidence zones for screening-level planning, whereas scenario-dependent areas indicate elevated uncertainty. This framework advances hydropower suitability assessment toward transparent, risk-aware, and adaptive spatial decision support in complex geothermal environments by shifting emphasis from single-model accuracy to scenario robustness and cross-method synthesis.

Keywords:

Decision Support;
Geothermal Regions;
Hydropower Planning;
Scenario-Based Analysis;
Spatial Suitability.

Article History:

Received:	09	January	2026
Revised:	03	May	2026
Accepted:	06	May	2026
Published:	01	June	2026

1- Introduction

The global transition toward low-carbon energy systems requires spatial planning frameworks that are transparent, robust, and capable of balancing energy production with ecological and regulatory constraints. Hydropower remains a strategic renewable resource in diversified energy portfolios due to its high conversion efficiency, long operational lifespan, and contribution to grid stability [1, 2]. Recent research on renewable energy planning emphasizes spatially explicit evaluation methods that integrate environmental sustainability and infrastructure feasibility within structured decision processes [3, 4]. However, the assessment of hydropower suitability in geodynamically complex regions remains analytically challenging because the hydraulic potential often coincides with high environmental sensitivity and regulatory constraints [5, 6].

Hydropower suitability mapping has traditionally relied on GI systems integrated with MCDA. Deterministic GIS approaches primarily estimate potential from elevation and discharge but do not explicitly differentiate planning

* **CONTACT**: saikhu@its.ac.id

DOI: https://doi.org/10.28991/ESJ-2026-010-03-09

scenarios [7]. MCDA frameworks, such as AHP, BWM, and fuzzy logic, integrate multiple thematic layers to generate composite suitability indices and are widely applied due to their interpretability and structured weighting logic [8, 9]. However, these approaches typically employ fixed or implicit weights within a single modeling paradigm and rarely assess how suitability outcomes vary across alternative analytical strategies, limiting their ability to support scenario-aware decision-making [10, 11].

Data-driven modeling has been increasingly introduced into spatial suitability analysis to reduce subjectivity and enhance predictive discrimination. ML approaches, including support vector machines and ensemble methods, have been used to improve the identification and spatial classification performance of dam sites [12, 13]. Gradient boosting models, such as XGBoost, demonstrate strong capability in capturing nonlinear relationships among multi-indicator spatial datasets [14]. Deep learning architectures, particularly convolutional neural networks, further enhance spatial representation by extracting contextual information from image patches [15, 16]. In parallel, unsupervised clustering techniques, such as K-means, have been applied to identify the spatial regimes of renewable energy zoning [17, 18]. Despite these advances, most studies apply these methods independently, without a controlled comparison under consistent scenario assumptions.

A critical gap remains. Existing studies rarely compare MCDA baselines directly with supervised boosting algorithms, RL clustering hybrids, and patch-based CNNs using identical data and scenario configurations. Scenario weighting adjustments are typically confined to a single modeling framework and are not consistently propagated across paradigms, which restricts cross-method robustness assessment [19, 20]. Moreover, classification accuracy is commonly prioritized while underrepresenting spatial coherence and cross-method agreement as indicators of decision reliability. This study explicitly addresses how the modeling paradigm and scenario weighting jointly influence hydropower suitability outcomes when MCDA, extreme gradient boosting, reinforcement learning hybrid k-means clustering, and patch-based CNNs are applied to identical, harmonized datasets [21].

The proposed framework is grounded in scenario-based spatial decision analysis, where scenarios represent structured expressions of alternative planning priorities rather than purely technical parameter adjustments [20]. The MCDA is employed as a knowledge-driven baseline that operationalizes explicit weight allocation across criteria groups. XGBoost is a supervised learning paradigm capable of modeling nonlinear interactions among terrain, hydrological, and regulatory variables [14]. Reinforcement learning hybrid k-means clustering combines unsupervised spatial grouping with adaptive optimization logic to explore regimes of intrinsic suitability beyond predefined labels [22, 23]. Patch-based CNNs incorporate neighborhood structure by processing local spatial windows, enabling improved spatial coherence of suitability patterns. Applying identical scenario weights across all paradigms isolates methodological behavior while preserving decision context consistency [15].

The study area is a geothermal-influenced region characterized by active tectonics, hydrothermal processes, and heterogeneous land-cover conditions [24, 25]. Hydropower planning in such environments must also consider the ecological risks and impacts of geothermal water discharge on the surrounding ecosystems. The area is deliberately selected as a critical development context where hydropower expansion intersects with geothermal dynamics and regulatory constraints, rather than as a case driven by data availability. This approach enables systematic evaluation of scenario sensitivity and spatial robustness under complex and policy-relevant conditions [26].

Six primary spatial features are selected through literature synthesis and domain relevance assessment rather than data-driven feature optimization. Slope and elevation represent terrain stability and hydraulic gradient conditions affecting infrastructure feasibility, respectively [27]. Vegetation index derived from satellite imagery captures ecological sensitivity and land-cover variability relevant to environmental compatibility [28, 29]. Land use and functional zoning encode anthropogenic regulation and spatial planning constraints [30]. Hydrological suitability integrates drainage and flow-related characteristics that are essential for energy generation [31]. To ensure transparency and consistency, the three planning scenarios are constructed using structured weighting procedures derived from established MCDA principles. A balanced scenario distributes weights proportionally across criteria, an environmental-priority scenario emphasizes vegetation and zoning constraints, and an energy-priority scenario amplifies hydrological and terrain suitability variables. Identical weights are applied across MCDA, XGBoost, RLKM, and PCNN to ensure that the observed spatial differences arise from the algorithmic structure rather than the scenario inconsistency [10].

Following established spatial coherence approaches, evaluation integrates conventional classification metrics with spatial robustness indicators, including fragmentation, spatial continuity, and cross-method agreement [21]. Independent regional-scale field validation data are not available; therefore, results are interpreted as comparative robustness analysis rather than absolute physical validation. This scope is explicitly defined to avoid overclaiming predictive certainty while strengthening methodological transparency. This study advances hydropower suitability mapping toward structured, scenario-aware spatial decision support in geothermal-influenced regions by explicitly addressing the research gap, theoretical positioning, feature justification, weighting transparency, and validation scope (see Table 1).

Table 1. Representative works related to hydropower suitability mapping and their limitations relative to the proposed framework [5, 7–12, 31–33]

No.	Study	Main Paradigm	Data Basis	Scenario Handling	Evaluation Focus	Key Strengths	Key Limitations
1	Tamm & Tamm [7]	GIS-based deterministic	DEM, discharge	None	Capacity verification	Simple, transferable, and low data demand	No scenario differentiation; ignores the environmental trade-offs
2	Odiji et al. [8]	GIS–AHP (MCDA)	Multithematic spatial layers	Implicit (fixed weights)	Suitability index	Transparent weighting; interpretable	Subjective weights: no robustness or spatial coherence assessment
3	Jafari et al. [10]	GIS–MCDM (BWM)	Terrain and hydrology	Single planning logic	Land suitability index (LSI)	Policy-relevant ranking	Single-scenario assumption with no cross-method comparison
4	Fasipe et al. [32]	GIS + hydrological modeling	DEM and flow models	None	Hydropower potential	Physically grounded estimation	Not suitability-oriented and lacks land-use constraints
5	Kucukali et al. [9]	GIS–Fuzzy MCDA	Dam and infrastructure data	Fixed	Suitability index	Handles uncertainty in the criteria	Case-specific; no scenario sensitivity analysis
6	Areri & Bibi [31]	GIS + AHP	DEM, stream network, and hydrological variables	Implicit	Site identification	Integrating GIS and hydrologic modeling	Limited Methodological Comparison
7	Paschetto et al. [5]	GIS + SWAT hydrological model	DEM, flow, and ecological flow constraints	None	Hydropower Potential with Ecological Compliance	Balance between energy production and ecosystem sustainability	Focus on potential estimation rather than comparative modeling
8	Mochani et al. [11]	Hybrid MCDA (AHP–ANP–Fuzzy)	Environmental, technical, and economic layers	Implicit	Priority ranking	Comprehensive criterion integration	Static weighting, no learning-based generalization
9	Akajiaku et al. [12]	MCDA + ML (SVM)	Geospatial and expert-labeled data	Limited	Accuracy vs. expert validation	Combining knowledge- and data-driven logic	Accuracy-centered; limited evaluation of spatial robustness
10	Rayat et al. [33]	Hybrid ML–DL	Multisource spatial datasets	Not explicit	Classification accuracy	High predictive performance	Black-box behavior and weak interpretability
11	This Study	Scenario-based MCDA vs. XGBoost vs. RL–KMeans vs. Patch-based CNN	Harmonized satellite-derived spatial layers	Explicit (S0–S2)	Cross-method agreement, spatial coherence, and robustness	Integrates interpretability, nonlinear learning, adaptive clustering, and contextual deep learning	Designed for decision support rather than absolute physical validation

2- Methodology

2-1- Framework Overview

This study develops a scenario-based interdisciplinary framework for hydropower site suitability mapping that integrates knowledge-driven decision analysis, supervised machine learning, unsupervised clustering, and spatially explicit deep learning within a unified decision-support structure (Figure 1). The framework is explicitly designed for planning-oriented analysis in geothermal-influenced and environmentally sensitive regions, where steep terrain, heterogeneous land cover, and regulatory constraints introduce substantial uncertainty into suitability assessments [11, 34].

Rather than optimizing a single predictive model or asserting absolute suitability accuracy, the methodological emphasis is placed on robustness, spatial coherence, and cross-method agreement as indicators of planning reliability [4, 13]. Consistent spatial patterns across alternative analytical paradigms are more informative for decision screening in data-limited and regulation-constrained contexts than marginal gains in model-specific performance metrics. All analytical components operate on harmonized spatial datasets with identical predictor variables and scenario definitions, ensuring that the observed differences in suitability outputs reflect methodological behavior and scenario assumptions rather than data inconsistencies [15, 35].

2-2- Characteristics of the Study Area

The study area is located within a geothermal-influenced region characterized by pronounced elevation variability, steep slopes, heterogeneous land use, and overlapping functional zoning regulations [39]. These characteristics create favorable hydraulic gradients for hydropower development while imposing strong constraints related to construction feasibility, environmental sensitivity, and land-use compatibility [40, 41]. The region is deliberately selected as a critical testbed rather than a typical development case, enabling the systematic evaluation of scenario sensitivity and spatial robustness under complex and competing planning conditions [4, 42]. Accordingly, the analytical objective is not site-specific optimization but the assessment of methodological robustness and scenario dependence in a policy-relevant planning environment.

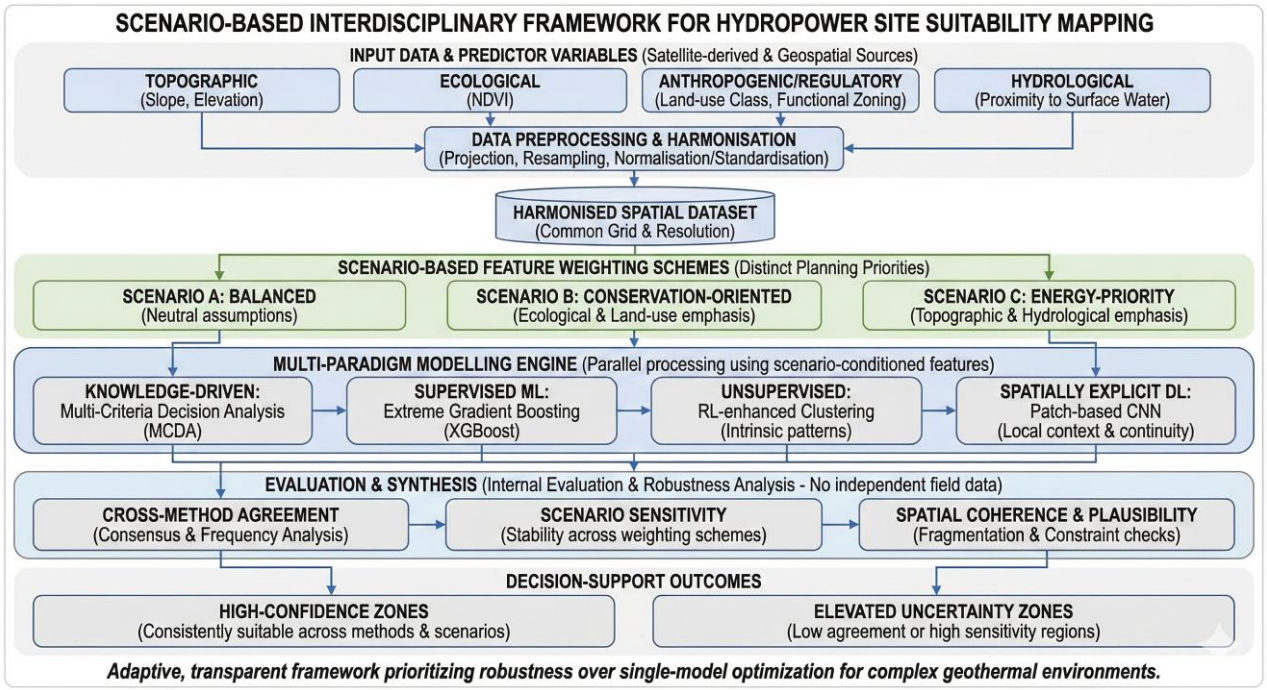

Figure 1. Overview of the Framework [4, 36–38]

2-3- Data Sources and Spatial Preprocessing

All spatial datasets used in this study were derived from publicly available satellite-based and geospatial sources, ensuring reproducibility and transferability. Six spatial predictor variables are employed: slope, elevation, Normalized Difference Vegetation Index (NDVI), land use, functional zone, and hydrological suitability [7, 31, 43]. Slope and elevation represent topographic controls on hydraulic potential and construction feasibility, respectively. NDVI serves as a proxy for vegetation density and ecological sensitivity, while land use and functional zone encode anthropogenic activity and spatial planning regulations. Hydrological suitability is a binary indicator that reflects the proximity to surface water features relevant to hydropower intake and flow continuity [5, 32, 44].

Feature selection is guided by hydropower planning literature, domain expertise, and data availability rather than data-driven optimization, ensuring interpretability and methodological transparency [16, 45]. All raster layers are harmonized to a common projection, spatial resolution, and grid [46]. Continuous variables (slope, elevation, and NDVI) are normalized using min–max scaling, categorical variables (land use and functional zone) are rescaled to standardized numeric ranges, and the native binary representation of hydrological suitability is retained (Table 2 and Figure 2). To preserve class semantics and analytical consistency across modeling approaches, training labels are excluded from normalization [13, 47].

Table 2. Spatial predictor variables, preprocessing strategy, and scenario-based weighting schemes are used [7, 31, 43]

No.	Spatial predictor	Conceptual Role in Hydropower Planning	Data type	Preprocessing and scaling	S0 (Balanced)	S1 (Conservation-oriented)	S2 (Energy-priority)
1	Slope	Hydraulic gradient control and construction feasibility	Continuous	Min–max normalization (0–1)	1.0	1.0	2.0
2	Elevation	Head potential and terrain constraints	Continuous	Min–max normalization (0–1)	1.0	1.0	2.0
3	Hydrological suitability	Proximity to surface water and flow continuity	Binary	Native binary scale (0/1)	1.0	1.0	2.0
4	Land use	Encodes anthropogenic activity and land-use restrictions	Categorical	Rescaled to the numeric range (0–1)	1.0	2.0	0.5
5	Functional zone	Spatial planning and regulatory constraints	Categorical	Rescaled to the numeric range (0–1)	1.0	1.0	2.0
6	NDVI	Proxy for Vegetation Density and Ecological Sensitivity	Continuous	Min–max normalization (0–1)	1.0	2.0	0.5

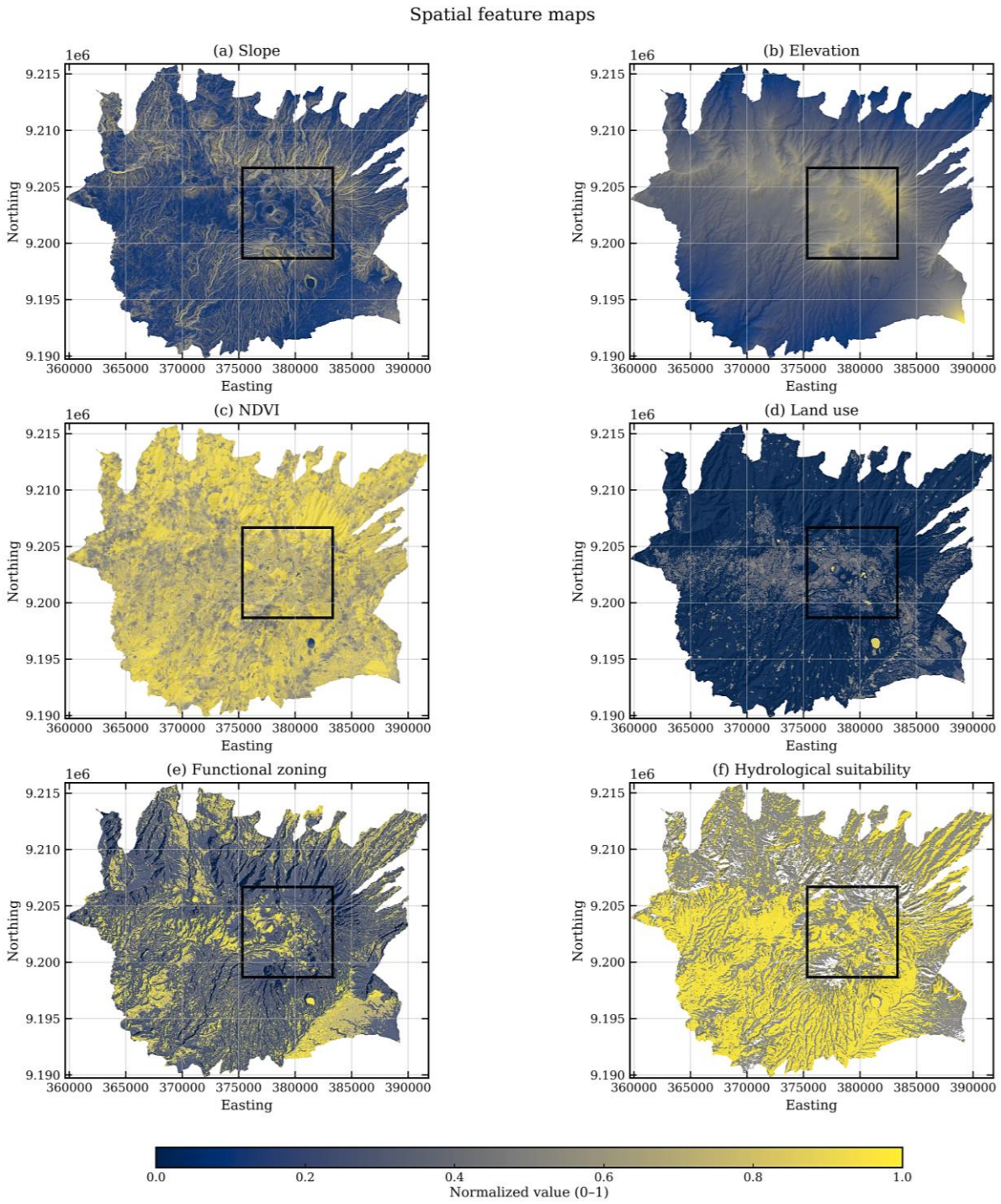

Figure 2. Spatial features with the black square region of interest representing the geothermal analysis area

2-4- Scenario Design

A scenario-based analysis constitutes a core component of the proposed framework (Table 2). A fixed set of SP variables is maintained across all scenarios, while differentiation is introduced exclusively through alternative feature-weighting schemes representing distinct planning priorities [48, 49]. Three scenarios have been defined [5, 50]: a balanced scenario (S0) with equal weighting across all predictors, a conservation-oriented scenario (S1) that emphasizes NDVI and land-use constraints, and an energy-priority scenario (S2) that emphasizes slope, elevation, hydrological suitability, and functional zone. The weighting schemes follow heuristic and literature-informed configurations, representing bounding planning perspectives rather than optimized or stakeholder-elicited solutions [51]. Scenario differentiation is applied solely to feature representations, whereas training labels remain unchanged. This design anchors learning processes to observed spatial patterns while allowing controlled exploration of alternative planning assumptions. The framework preserves methodological transparency and avoids over-claiming predictive validity in the absence of independent field validation by applying identical predictor sets and explicit weighting schemes across all analytical paradigms [52].

2-5- Data-Driven Modeling for Hydropower Suitability

2-5-1- MCDA as the Baseline

Multi-Criteria Decision Analysis is employed as a knowledge-driven and deterministic baseline for hydropower suitability mapping. Scenario-specific weights are applied to the normalized spatial predictors, and weighted linear aggregation is used to compute suitability scores [11, 34].

$$S_i = \sum_{j=1}^{n} w_j \; x_{ij} \tag{1}$$

here, x_{ij} is the normalized value of predictor j at pixel i, w_j is the scenario-specific weight, and n is the number of predictors. MCDA does not aim to maximize predictive accuracy; instead, it provides a transparent reference surface that explicitly encodes planning assumptions. Therefore, MCDA outputs are used to support the evaluation of spatial coherence, scenario sensitivity, and agreement with data-driven approaches rather than to define ground-truth suitability [10, 49].

2-5-2- Extreme Gradient Boosting (XGBoost)

Extreme Gradient Boosting is applied as a supervised learning approach to capture nonlinear relationships among spatial predictors. Scenario differentiation is implemented by applying scenario-specific weights to the feature stack before training and inference to ensure consistency with the scenario framework [12, 14]. Identical training samples, data partitions, and preprocessing procedures are used across scenarios to isolate planning-priority effects from the model configuration. The model behavior is evaluated using standard classification metrics and feature importance analysis [13, 47].

2-5-3- RLKM

A reinforcement learning–enhanced K-Means clustering approach is employed to explore the intrinsic spatial patterns under limited labeled data conditions. Cluster centroids are refined iteratively using a reward mechanism that promotes spatial compactness and internal consistency [17, 53]. Scenario-specific feature weighting is applied before clustering, allowing planning priorities to influence cluster formation without modifying training labels. This unsupervised approach reveals that rather than predefined class assignments, suitability regimes emerge from spatial structure [22, 54].

2-5-4- Patch-Based CNN (PCNN)

A patch-based CNN is implemented to explicitly incorporate the local spatial context. By processing fixed-size spatial patches rather than individual pixels, neighborhood interactions and spatial continuity are captured [15, 16]. Scenario differentiation is applied using weighted feature patches, ensuring consistency with the scenario design. This spatially explicit DL approach reduces output fragmentation and produces more contiguous suitability zones for screening-level hydropower planning [33, 47].

2-6- Internal Evaluation and Spatial Robustness

2-6-1- Cross-Method Agreement

Cross-method agreement is used to evaluate the consistency of suitability outcomes across analytical paradigms. Binary suitability maps from MCDA, supervised learning, unsupervised clustering, and deep learning are pixel-by-pixel compared using a common grid. Agreement frequency at pixel is defined as follows:

$$A_i = \sum_{m=1}^{M} b_{im} \tag{2}$$

where, $b_{im} \in \{0,1\}$ denotes the binary output of method m, and M denotes the number of methods. Pixels with high agreement values indicate methodological convergence and are interpreted as candidates with robust screening-level [30, 55]

2-6-2- Scenario Sensitivity

The stability of suitability patterns under alternative planning priorities (S0–S2) is assessed by scenario sensitivity. Changes in feature-weighting schemes are used to examine how spatial outcomes respond to decision assumption shifts. Areas exhibiting consistent suitability across scenarios are interpreted as scenario-robust, whereas unstable areas indicate sensitivity to planning priorities, supporting comparative scenario interpretation rather than PPA [56, 57].

2-6-3- Spatial Coherence and Plausibility

Spatial coherence and plausibility were evaluated to assess the practical interpretability of the outputs. Fragmentation metrics, including patch count and average patch size, are used to quantify the spatial continuity. Suitability maps are

further screened against physical and functional constraints, such as slope thresholds, hydrological proximity, and zoning regulations. Integrating coherence metrics with constraint checks ensures that the identified suitability zones are spatially contiguous and compatible with real-world planning conditions [58].

3- Results

3-1- Overall Suitability Patterns across S0–S2 Hydropower Planning Scenarios

The MCDA-based suitability maps reveal systematic yet spatially constrained responses to scenario-specific weighting schemes (Figure 3). Transitioning from the balanced scenario (S0) to conservation-oriented (S1) and energy-priority (S2) configurations primarily affects marginal suitability zones, whereas core suitable areas remain spatially persistent. This behavior is consistent with previous GIS–MCDA studies, where scenario-based reweighting predominantly modifies transitional areas rather than redefining the spatial core of suitability outcomes [4, 30]. Table 3 indicates a progressive reduction in the fraction of suitable pixels from 20% under S0 to 17.68% in S1 and 15.71% in S2, corresponding to net changes of −2.32% and −4.29%, respectively. These shifts reflect the intended influence of scenario priorities, whereby conservation-oriented weighting constrains marginally suitable areas, whereas energy-priority configurations apply stricter suitability thresholds without expanding the overall suitable footprint. Similar patterns of areal contraction and boundary sensitivity under alternative weighting schemes have been reported in scenario-based hydropower site selection and spatial MCDA applications [11, 27].

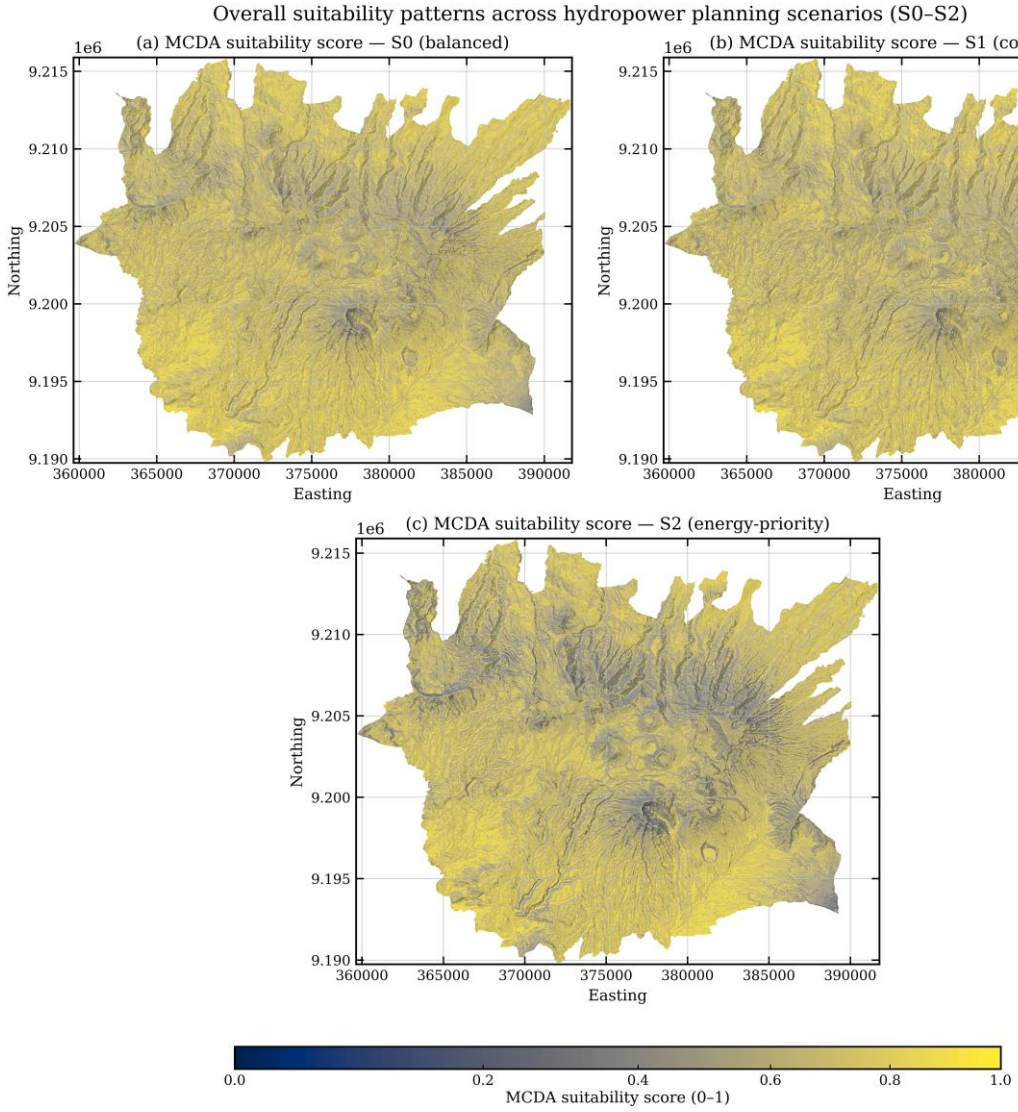

Figure 3. MCDA baseline suitability maps across the S0–S2 range [4, 36–38]

The observed spatial differences are interpreted as planning-priority effects rather than indicators of real-world site optimality. The MCDA outputs serve as comparative screening maps that illustrate how suitability distributions respond to alternative assumptions and policy orientations, rather than as validated predictions of hydropower feasibility [4]. This framing positions the scenario-based results as tools for sensitivity exploration and spatial decision support under uncertainty, consistent with best practices in RE planning.

Table 3. Areal distribution of suitable zones across the MCDA planning scenarios (S0–S2)

No.	Spatial indicator	S0 (Balanced)	S1 (Conservation-oriented)	S2 (Energy-priority)
1	Fraction of the suitable pixels	0.20	0.18	0.16
2	Percentage of the study area	20	17.68	15.71
3	Net change relative to S0 (%)	0	−2.32	−4.29

3-2- Baseline and Data-Driven Suitability Patterns Under a Reference Scenario

To establish a consistent reference for cross-method comparison, suitability outputs from MCDA and DDMs are examined under an identical scenario setting (S0), using harmonized inputs and thresholds (Figure 4). Under this reference configuration, MCDA produces smoother and more spatially continuous suitability patterns, reflecting its weighted aggregation structure and role as a KDS baseline. Comparable smoothing behavior has been widely reported in GIS-MCDA applications for hydropower and renewable energy planning, where spatial continuity is an inherent consequence of additive weighting schemes rather than a predictive objective [4, 30].

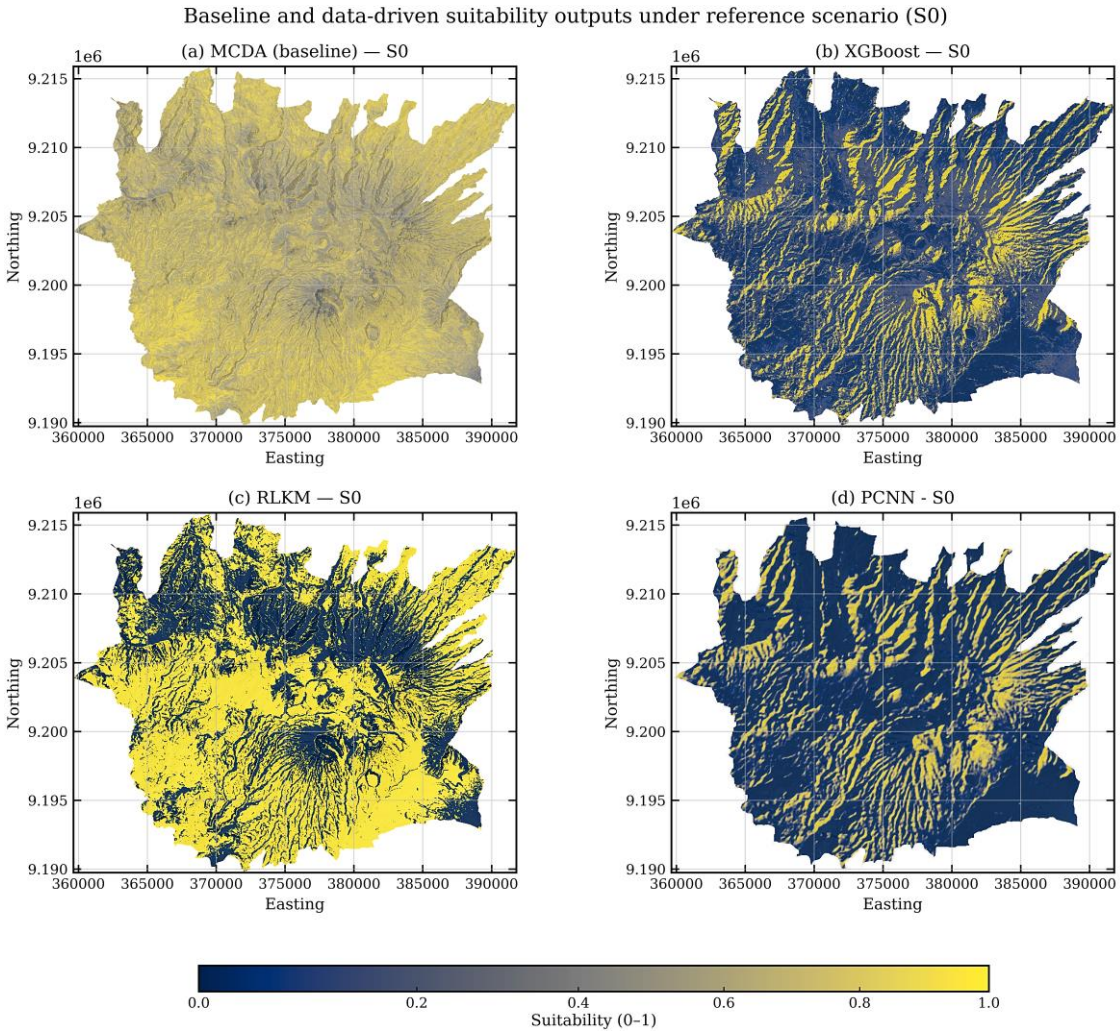

Figure 4. Suitability outputs under S0 for the baseline and selected models [4,36–38]

In contrast, supervised and DL models display sharper spatial contrasts and more fragmented suitability boundaries. The XGBoost output highlights narrow linear features and localized high-suitability zones, consistent with its capacity to model non-linear interactions among terrain and environmental predictors [12, 14]. The PCNN result further amplifies spatial coherence along physiographic structures through neighborhood-based feature learning, a behavior commonly observed in CNN-based geospatial suitability and susceptibility mapping [15, 33]. The RLKM output exhibits comparatively compact and clustered suitability regions, reflecting its unsupervised learning mechanism that groups areas based on intrinsic feature similarity rather than externally defined suitability labels. Similar clustering-driven spatial compartmentalization has been documented in unsupervised and hybrid clustering approaches applied to renewable energy siting, where suitability emerges from feature homogeneity rather than explicit decision criteria [17, 53].

Importantly, these visual contrasts are interpreted as differences in methodological behavior under a common scenario, not as indicators of physical correctness or real-world feasibility. Therefore, the comparison under S0 functions as a qualitative bridge to subsequent internal evaluation, illustrating how alternative analytical paradigms redistribute suitability when exposed to identical assumptions. This interpretation aligns with best practices in scenario-based spatial planning, where baseline comparisons are used to reveal model sensitivity and complementarity rather than to assert model superiority [4].

3-3- Internal Evaluation and Spatial Robustness Analysis

3-3-1- Cross-Method Agreement

Cross-method agreement was employed to assess the internal robustness of suitability patterns by examining the spatial consensus among different analytical paradigms under identical scenario settings (Figure 5). This analysis identifies locations where suitability classification is stable across methodological assumptions rather than serving as empirical validation, providing a reliable signal for screening-level decision support. Similar consensus-oriented approaches have been widely adopted in spatial planning studies where independent ground-truth data are unavailable [4, 30, 59].

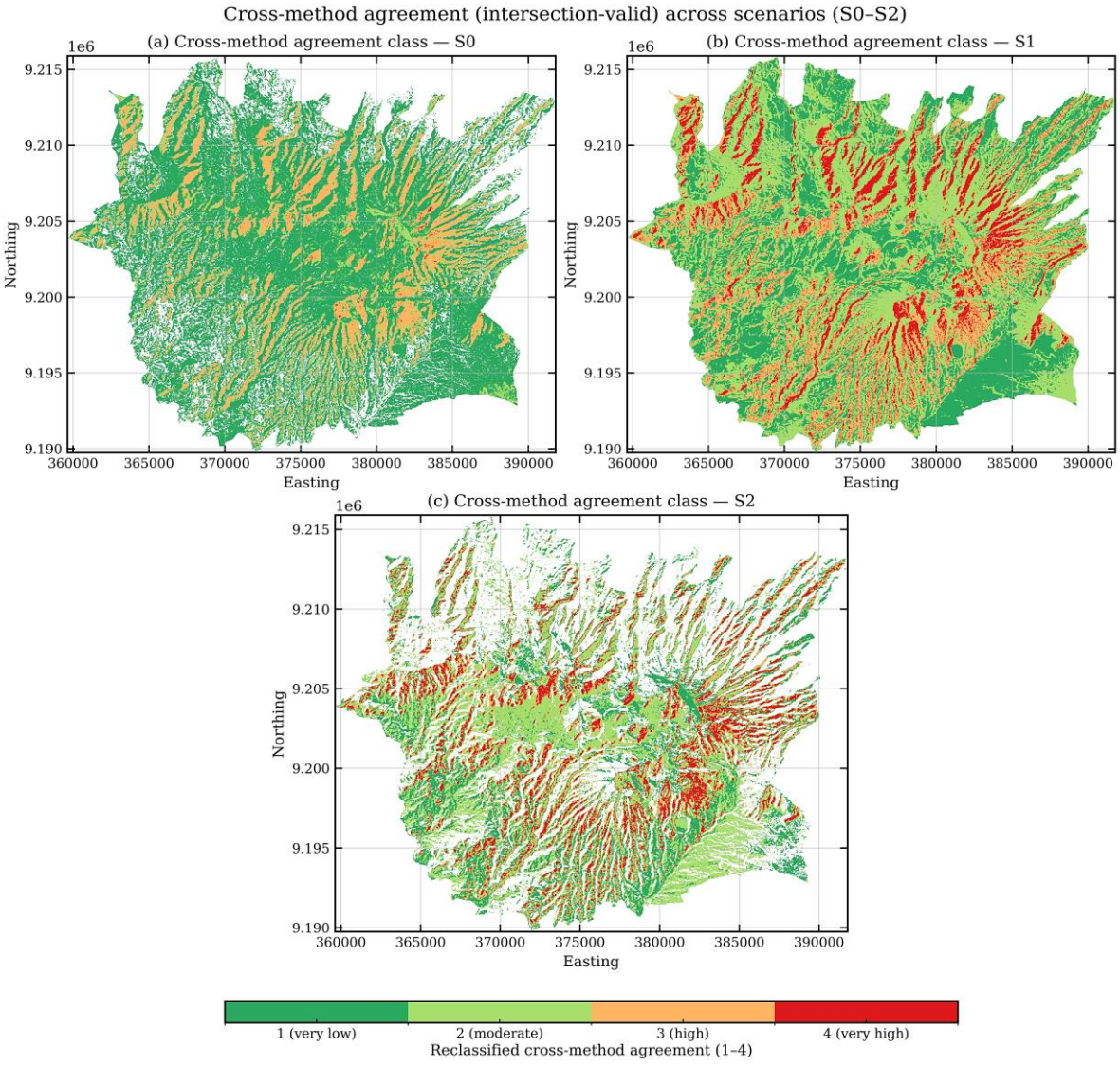

Figure 5. Cross-method agreement was observed [4, 36–38]

Across all scenarios (S0–S2), supermajority agreement (≥3 out of 4 methods) within union-valid areas remains maximal (Table 4), indicating that their suitability classifications are highly consistent where multiple model outputs spatially overlap. However, the proportion of intersection-valid pixels relative to the union-valid extent is limited (3.44%–5.26%), reflecting scenario-driven expansion and contraction of suitable areas rather than disagreement among methods. This pattern differences primarily influence the spatial reach of suitability zones, while core agreement areas remain stable across analytical paradigms.

Table 4. Cross-method agreement plus summary per scenario (union- and intersection-valid)

No.	Scenario	Methods Used	Union-Valid Pixels	Intersection-Valid Pixels	Intersection/ Union (%)	Supermajority Agreement (≥3 methods) – Union-Valid	Supermajority Pixels (Intersection)	Fraction ≥3 Agreement (Intersection)
1	S0	MCDA, XGBoost, RLKM, and PCNN	570,659	34,388	3.87	1.00	34,388	1.00
2	S1		570,658	46,752	5.26	1.00	46,752	1.00
3	S2		570,655	30,517	3.44	1.00	30,517	1.00

A value of 1.00 indicates that all intersection-valid pixels satisfy the ≥3-method agreement criterion; however, this does not imply full-area agreement.

Vote distribution analysis further supports this interpretation, with all intersection-valid pixels exhibiting complete agreement (4/4 votes) across MCDA, XGBoost, RLKM, and PCNN under all scenarios (Table 5). Such unanimous agreement is interpreted as a strong indicator of internal consistency, highlighting zones where suitability classification is robust to model choice. Consistent with best practices in GIS-based MCDA and data-driven suitability mapping, this form of consensus mapping is intended to support confidence-based prioritization rather than implying physical correctness or real-world feasibility [27, 60]. Vote distribution is reported only for intersection-valid pixels to ensure comparability across methods.

Table 5. Vote distribution of suitability agreement across methods per scenario

No.	Scenario	Number of methods (M)	0/4 Votes	1/4 Votes	2/4 Votes	3/4 Votes	4/4 Votes
1	S0	4	0.00	0.00	0.00	0.00	1.00
2	S1	4	0.00	0.00	0.00	0.00	1.00
3	S2	4	0.00	0.00	0.00	0.00	1.00

3-3-2- Scenario Sensitivity

Scenario sensitivity analysis evaluates how internal performance indicators respond to changes in planning priorities across scenarios S0–S2 to distinguish scenario-robust from weight-sensitive modeling behaviors (Tables 6 and 7). The reported metrics are derived from reference or proxy samples and are used exclusively for relative sensitivity assessment, not for external predictive validation. This approach is consistent with established practices in spatial decision-support studies where independent ground-truth data are unavailable [4, 30].

Table 6. Internal performance (reference samples) across the methods and scenarios

Method	Scenario	Accuracy	Precision	Recall	F1-score	Specificity	ROC–AUC
MCDA	S0	0.500	0.500	1.000	0.667	0.000	0.378
MCDA	S1	0.500	0.500	1.000	0.667	0.000	0.360
MCDA	S2	0.500	0.500	1.000	0.667	0.000	0.368
XGBoost	S0	0.909	0.935	0.879	0.906	0.939	0.960
XGBoost	S1	0.909	0.935	0.879	0.906	0.939	0.960
XGBoost	S2	0.909	0.935	0.879	0.906	0.939	0.960
PCNN	S0	0.915	0.887	0.952	0.918	0.877	0.964
PCNN	S1	0.905	0.886	0.931	0.908	0.879	0.961
PCNN	S2	0.912	0.891	0.941	0.915	0.883	0.964
RLKM	S0	0.576	0.603	0.449	0.515	0.703	0.576
RLKM	S1	0.542	0.540	0.570	0.554	0.513	0.542
RLKM	S2	0.557	0.581	0.410	0.481	0.704	0.557

Table 7. Scenario robustness score across methods and metrics

Method	Metric	S0	S1	S2	Scenario robustness score
MCDA	Accuracy	0.500	0.500	0.500	1.000
MCDA	F1-score	0.667	0.667	0.667	1.000
MCDA	ROC–AUC	0.378	0.360	0.368	0.988
XGBoost	Accuracy	0.909	0.909	0.909	1.000
XGBoost	F1-score	0.906	0.906	0.906	1.000
XGBoost	ROC–AUC	0.960	0.960	0.960	1.000
PCNN	Accuracy	0.915	0.905	0.912	0.994
PCNN	F1-score	0.918	0.908	0.915	0.993
PCNN	ROC–AUC	0.964	0.961	0.964	0.998
RLKM	Accuracy	0.576	0.542	0.557	0.977
RLKM	F1-score	0.515	0.554	0.481	0.951
RLKM	ROC–AUC	0.576	0.542	0.557	0.977

Supervised paradigms (XGBoost and PCNN) exhibit highly stable internal performance across all scenarios, with identical or near-identical values for accuracy, F1-score, and ROC–AUC. This stability indicates that model outputs are largely insensitive to scenario reweighting, indicating robustness to planning assumption shifts. Similar behavior has been reported in data-driven spatial suitability studies, where supervised models tend to preserve relative performance under alternative weighting configurations when trained on harmonized feature sets [13, 60].

MCDA displays invariant performance metrics across scenarios due to its deterministic formulation and rule-based structure. The characteristic pattern of perfect recall and zero specificity reflects the inherent binary thresholding logic of MCDA-based screening rather than predictive capability. Therefore, these metrics are interpreted as the method's structural properties, reinforcing its role as a baseline decision framework rather than a performance-optimized classifier. In contrast, RLKM demonstrates noticeable variability across scenarios, particularly in recall, F1-score, and ROC–AUC values. This variability indicates sensitivity to weighting assumptions, consistent with the exploratory nature of unsupervised and reinforcement-driven clustering approaches, where feature weighting and scenario emphasis directly influence cluster formation and class separation [18, 53].

To synthesize scenario sensitivity across metrics, the SRS is introduced as a composite indicator of performance consistency across S0–S2 (Table 7). High SRS values for XGBoost and PCNN confirm scenario-robust behavior, whereas lower SRS values for RLKM indicate weight-sensitive responses. These results support a functional classification of analytical paradigms according to their robustness to planning assumptions rather than ranking models by accuracy, which informs their complementary roles in subsequent decision-support synthesis [61, 62].

3-3-3-Spatial Coherence and Plausibility

Spatial coherence analysis is used to evaluate whether suitability outputs form contiguous and interpretable spatial patterns that are meaningful for screening-level hydropower planning, independent of predictive performance metrics. Fragmentation statistics (Table 8) reveal pronounced contrasts among analytical paradigms, highlighting the influence of methodological design on the spatial readability and stability of suitability maps. This analysis follows the established literature on spatial planning, emphasizing that highly fragmented suitability outputs may limit interpretability and practical applicability despite strong classification performance [4, 30].

Table 8. Summary of fragmentation using method and scenario

Method	Scenario	Average patch size (pixels)	Number of patches	Fraction of the large patches
MCDA	S0	95,109.67	6	0.99995
MCDA	S1	95,108.17	6	0.99995
MCDA	S2	95,108.50	6	0.99995
XGBoost	S0	16.81	5,754	0.64832
XGBoost	S1	16.81	5,754	0.64832
XGBoost	S2	16.81	5,754	0.64832
RLKM	S0	37.67	6,222	0.85099
RLKM	S1	81.16	4,730	0.95650
RLKM	S2	36.55	6,306	0.84806
PCNN	S0	161.88	875	0.90055
PCNN	S1	156.00	880	0.90284
PCNN	S2	148.75	906	0.89998

MCDA consistently produces extremely large and contiguous suitable zones with minimal fragmentation across all scenarios, reflecting its smooth aggregation and rule-based structure. In contrast, XGBoost generates highly fragmented spatial patterns characterized by thousands of small patches and small average patch size, indicating strong local sensitivity to feature gradients. Although such fine-grained discrimination may be advantageous for predictive tasks, it can reduce map legibility and complicate early-stage planning interpretation when applied without spatial regularization [13, 27]. RLKM exhibits intermediate fragmentation behavior with clear scenario-dependent variability, indicating sensitivity to weighting assumptions and internal clustering dynamics. In contrast, PCNN consistently reduces patch fragmentation relative to pixel-based supervised outputs, producing larger and more coherent suitability zones across scenarios. This behavior reflects the influence of neighborhood-based feature learning, which enhances spatial continuity while preserving discriminative structure [15, 33]

Importantly, the spatial coherence indicators are interpreted comparatively rather than absolutely, without reference to the actual dam size or engineering feasibility. The results demonstrate that high predictive discrimination alone does not guarantee spatial plausibility and that contiguity and pattern stability are critical attributes for screening-level decision support. Consequently, rather than inferring real-world optimality, spatial coherence metrics are used to distinguish modeling approaches that yield more readable and stable suitability patterns under scenario uncertainty.

3-4- Consolidated Summary of Evidence for Robust Planning Interpretation

Internal evidence is consolidated across three complementary dimensions to avoid overreliance on a single evaluation axis: (i) performance stability across scenarios, (ii) cross-method spatial consensus, and (iii) spatial coherence of suitability patterns. Supervised paradigms (XGBoost and PCNN) demonstrate high and stable internal performance across all scenarios, confirming robustness to scenario weighting assumptions, a behavior commonly observed in supervised spatial modeling under harmonized inputs [60]. However, PCNN consistently improves spatial coherence relative to pixel-based XGBoost outputs, reducing fragmentation and enhancing the contiguity of suitable zones through neighborhood-aware feature learning [15]. MCDA provides the most interpretable and spatially contiguous baseline behavior but remains strictly assumption-driven and does not represent empirical ground truth, consistent with its established role in decision-support screening rather than predictive validation [30]. RLKM contributes a complementary regime-based perspective, exhibiting moderate robustness and sensitivity to scenario reweighting, as commonly reported for unsupervised and clustering-based spatial analyses [53].

This consolidated evidence (Table 9) indicates that robust screening-level suitability maps emerge from multi-criteria internal consistency, rather than from single-model optimization or isolated accuracy metrics, aligning with contemporary spatial planning frameworks that emphasize robustness and interpretability over pointwise predictive performance [20]. Importantly, all indicators are derived from proxy-based internal evaluation and valid-only spatial analysis and are therefore interpreted comparatively for decision-support screening rather than as external predictive validation.

Table 9. Consolidation of internal evidence across methods (performance, agreement, spatial coherence, and robustness)

Method	Performance stability (↓ better)	Cross-method coverage	Average patch size (pixels)	Mean number of patches	Large-patch fraction	Mean scenario robustness
MCDA	0.0030	0.642	95,108.78	6	0.99995	0.996
XGBoost	0.0000	0.109	16.81	5,754	0.64832	1.000
RLKM	0.0238	0.319	51.79	5,753	0.88519	0.968
PCNN	0.0039	0.155	155.54	887	0.90112	0.995

3-5- Synthesis of Decision Support Mapping Results

Collectively, the results demonstrate that no single analytical paradigm should be treated as universally optimal under scenario uncertainty. Instead, decision-support mapping benefits from integrating complementary evidence: MCDA encodes transparent planning assumptions, supervised learning provides discriminative capability, unsupervised clustering reveals intrinsic spatial regimes, and deep learning enhances spatial coherence [30]. High-confidence zones are operationally defined as areas supported by cross-method consensus and low scenario sensitivity, whereas scenario-sensitive zones are interpreted as policy-dependent and require cautious use, consistent with scenario-based spatial planning practices [63]. This synthesis positions the resulting suitability maps as screening-level decision support, explicitly addressing the lack of independent field validation.

4- Discussion

4-1- Interpretation of Stability Suitability in a Geothermal-Influenced Context

The scenario-based MCDA results (Figure 3 and Table 3) indicate that the suitability contraction from S0 (20%) to S1 (17.68%) and S2 (15.71%) primarily affects marginal zones rather than core suitability clusters. This behavior is theoretically consistent with structured multi-criteria planning frameworks, where weight adjustments reshape boundary

areas while preserving high-gradient hydraulic corridors [4, 30]. Such persistence of core zones in geothermal-influenced terrain characterized by steep slopes, tectonic activity, and heterogeneous land use that topographic–hydrological controls dominate baseline spatial feasibility [24, 41]. From a hydropower planning perspective, this implies that certain physiographic corridors remain consistently favorable regardless of policy emphasis, whether conservation-oriented or energy-priority. This does not imply engineering feasibility or economic viability [43, 64]. Rather, geomorphological suitability patterns are structurally robust to moderate planning-weight perturbations. This distinction is critical in geothermal regions where hydrothermal discharge, subsurface instability, and land-use regulation may introduce additional non-modeled constraints [26]. Thus, the contraction observed in Table 3 should be interpreted as policy filtering rather than resource depletion. Conservation-oriented weighting suppresses ecologically sensitive zones (NDVI- and land-use-dominated areas), whereas energy-priority weighting tightens hydraulic-gradient constraints [65]. The persistence of central clusters across scenarios supports the argument that scenario-robust screening zones can be identified even under complex geothermal–environmental interactions [66, 67].

4-2- Methodological Behavior: What the Paradigms Actually Do

Methodological differences become explicit under the common reference scenario (S0) (Figure 4). MCDA produces smooth and contiguous suitability patterns due to additive aggregation logic, consistent with the GIS–MCDA behavior documented in the literature on renewable energy siting (Table 1) [5, 7–12, 31–33]. In contrast, XGBoost emphasizes local nonlinear interactions, generating sharper boundaries and highly fragmented patches (Table 8). The fragmentation statistics provide quantitative evidence of this contrast (Table 8). XGBoost produce 5,754 patches with an average size of 16.81 pixels, whereas MCDA generates only six large contiguous patches. PCNN substantially reduces fragmentation (875–906 patches depending on the scenario) while maintaining high predictive discrimination (Table 6). This demonstrates that spatial context integration materially improves map readability and spatial coherence, which are essential attributes for screening-level planning [60, 68, 69]. The RLKM exhibits intermediate fragmentation and noticeable scenario sensitivity (Tables 7 and 8). This reflects the unsupervised nature: cluster formation, which is directly influenced by weighted feature space geometry [70, 71]. Such sensitivity is expected rather than problematic in geothermal terrains where environmental and hydraulic indicators may conflict spatially [72, 73]. Therefore, RLKM serves as an exploratory diagnostic tool, revealing weight-sensitive spatial regimes rather than delivering performance-optimized classification [74]. These behavioral distinctions are not framed as claims of superiority. Instead, they demonstrate that the algorithmic structure materially shapes the spatial morphology. This directly addresses the question of methodological comparability: all models use identical predictors and scenario weights (Table 2), whereas differences in output arise from intrinsic modeling assumptions and not from inconsistent pre-processing [75].

4-3- Cross-Method Agreement as a Robust Signal

The cross-method agreement analysis (Figure 5 , Tables 4 and 5) reveals that all intersection-valid pixels satisfy ≥3-method consensus, with a unanimous 4/4 agreement in those zones. Importantly, the intersection-valid coverage represents only 3.44%–5.26% of the union-valid extent. This pattern has two critical implications. First, zones of unanimous agreement represent high-confidence screening candidates [76]. In these areas, deterministic weighting, supervised nonlinear modeling, clustering structure, and contextual deep learning converge. In terms of decision support, such convergence reduces the epistemic uncertainty associated with model selection . Second, the relatively small intersection proportion indicates that the methodological complementarity remains substantial. The absence of disagreement within intersection areas does not imply universal agreement across the landscape; it simply shows that consensus is complete where overlap exists. This nuance avoids over claiming predictive certainty and aligns with best practice cautions in the literature on spatial validation [59]. For geothermal regions, where subsurface processes and hydrothermal discharge may introduce latent constraints, reliance on cross-method convergence rather than single-model optimization provides a more conservative planning signal. Therefore, consensus-based screening strengthens robustness without requiring physical validation [77].

4-4- Scenario Robustness Versus Weight Sensitivity

The Scenario Robustness Scores (Table 7) show near-perfect stability for XGBoost and PCNN across S0–S2, whereas RLKM displays moderate variability (mean SRS 0.968). The invariance of MCDA reflects deterministic rule application rather than empirical adaptability [4, 36, 38]. The stability of the supervised paradigms, that nonlinear feature interactions dominate over moderate weight adjustments. In practice, this means that once trained on harmonized predictors, boosted trees and CNN architectures preserve discriminative structure even when planning emphasis shifts [15, 78]. However, robustness should not be equated with realism. Stable metrics do not confirm external validity. They indicate internal consistency under controlled perturbations. This interpretation addresses the scope of validation: no independent field validation dataset is available; therefore, all performance indicators (Table 6) represent relative internal robustness and not actual empirical truth [59, 79].

4-5- Spatial Coherence and Readability of Planning

Fragmentation analysis (Table 8) demonstrates that the predictive performance alone does not guarantee spatial plausibility [60, 80]. XGBoost achieves a high ROC–AUC (0.960; Table 6) but produces highly fragmented outputs.

PCNN achieves comparable discrimination (ROC–AUC up to 0.964) while substantially increasing the average patch size (148–162 pixels) [81, 82]. Spatial readability and contiguity are critical for screening-level hydropower planning. Infrastructure siting requires contiguous corridors rather than isolated pixels. Therefore, PCNN's contextual learning provides a meaningful structural advantage without altering scenario robustness. MCDA produces extremely large contiguous zones (average patch size ≈95,000 pixels; Table 8), which enhances interpretability but oversmooths transitional areas. Thus, MCDA is best interpreted as a transparent assumption-driven baseline, PCNN as a spatially coherent discriminator, XGBoost as a high-resolution interaction detector, and RLKM as a regime-sensitive exploratory tool. This complementary interpretation prevents methodological overclaiming and reframes model diversity as epistemic triangulation rather than competition [83–86].

4-6- Implications for Hydropower Screening in Geothermal Regions

The geothermal context introduces additional complexity beyond conventional hydropower suitability mapping because active tectonics, hydrothermal discharge processes, and overlapping regulatory zoning frameworks require that spatial outputs be strictly interpreted as screening-level feasibility rather than development approval [4, 87]. Within this context, the identification of scenario-robust and cross-method-consensus zones indicates that certain physiographic suitability patterns remain stable even when environmental priorities are strengthened [88]. Conversely, areas that fluctuate under conservation-oriented weighting (Table 3) reveal potential ecological conflict zones, particularly where NDVI and land-use constraints exert a stronger influence. Accordingly, the framework contributes by systematically differentiating robust corridors characterized by high cross-method agreement and low scenario sensitivity, policy-sensitive zones shaped by weight-dependent suitability shifts and method-sensitive regimes revealed through RLKM variability [89]. This structured differentiation is consistent with the adaptive spatial planning theory, in which uncertainty is explicitly recognized and incorporated into decision-support processes rather than being artificially minimized [74].

4-7- Positioning Relative to Previous Studies

Previous hydropower suitability studies have predominantly relied on single-paradigm MCDA frameworks or accuracy-oriented machine learning approaches, with limited emphasis on propagating identical scenario-weighting schemes across multiple modeling paradigms for controlled robustness comparison (Table 1) [5, 7–12, 31–33]. In contrast, the present study does not position its contribution in terms of higher predictive accuracy, but in demonstrating that scenario reweighting primarily modifies marginal zones rather than core physiographic corridors (Table 3), that cross-method consensus offers a more meaningful robustness signal than isolated ROC–AUC metrics (Tables 4 to 6), and that spatial coherence indicators (Table 8) substantially influence planning interpretability beyond classification performance [90]. This framework addresses a research gap by explicitly analyzing how modeling paradigms and scenario weightings jointly shape suitability stability under geothermal complexity and reframes suitability mapping from single-model optimization to structured resilience assessment [91, 92].

5- Conclusion

This study developed and systematically evaluated a scenario-based multi-paradigm framework for hydropower suitability mapping in a geothermal-influenced region by directly comparing MCDA, XGBoost, RLKM, and patch-based CNN under harmonized datasets and identical weighting schemes. The results demonstrate that scenario reweighting primarily reshapes marginal suitability boundaries, whereas core physiographic corridors remain spatially persistent across conservation-oriented and energy-priority configurations. This stability confirms the structural dominance of terrain–hydrological controls in defining the spatial feasibility of the baseline. Cross-method agreement analysis reveals complete consensus within intersection-valid areas, indicating that methodological convergence rather than isolated model performance results in robustness. Supervised paradigms exhibit near-perfect scenario robustness, whereas RLKM captures weight-sensitive spatial regimes, highlighting its diagnostic value in revealing the assumption-dependent structure. Spatial coherence analysis shows that predictive discrimination alone does not ensure planning interpretability: neighborhood-based DL substantially reduces fragmentation and improves spatial contiguity without compromising robustness.

From a decision-support perspective, the framework enables structured differentiation between scenario-robust corridors, policy-sensitive transition zones, and method-sensitive regimes. Such differentiation is particularly critical in geothermal contexts where tectonic instability, hydrothermal discharge, and overlapping zoning regulations necessitate conservative screening logic. Rather than asserting development optimality, the proposed approach provides transparent robustness signals that strengthen early-stage feasibility assessment and adaptive planning strategies under uncertainty.

This study reframes hydropower suitability mapping from single-model optimization toward structured robustness assessment by integrating scenario sensitivity, cross-method consensus, and spatial coherence. Future research should incorporate independent field validation, dynamic hydrological discharge modeling, geothermal–hydropower interaction datasets, and formal uncertainty quantification to further enhance empirical grounding and transferability across heterogeneous RE landscapes.

5-1- Limitations

Several limitations must be acknowledged to avoid overinterpretation of the results. No independent field validation dataset was available; therefore, all evaluation metrics represent internal robustness indicators rather than empirical confirmation of real-world hydropower feasibility. Feature selection was guided by literature synthesis and domain expertise rather than statistical optimization, which strengthens interpretability but may exclude locally significant geothermal subsurface indicators. Instead of incorporating dynamic discharge modeling, hydrological suitability was simplified as a proximity-based indicator, and geothermal–hydropower interactions were represented indirectly through spatial proxies rather than through coupled hydrothermal simulations. Accordingly, the outputs should be strictly interpreted as structured decision-support screening products and not as engineering feasibility assessments or development approvals.

6- Declarations

6-1- Author Contributions

Conceptualization, A.S. and I.M.A.; methodology, A.S. and I.M.A.; software, R.F.I.; validation, R.F.I.; formal analysis, R.F.I.; investigation, R.F.I.; resources, X.X.; data curation, A.S. and I.M.A.; writing—original draft preparation, A.S. and I.M.A.; writing—review and editing, A.S., I.M.A., and W.U.; visualization, R.F.I.; supervision, A.S., I.M.A., and W.U. All authors have read and agreed to the published version of the manuscript.

6-2- Data Availability Statement

The data supporting the findings of this study are available from the corresponding author upon reasonable request.

6-3- Funding

This research was supported by the Center for Artificial Intelligence and Digital Technology (KATD), Institut Teknologi Sepuluh Nopember (ITS). The authors gratefully acknowledge financial support from the Fundamental Regular Research (PFR) Scheme of the Directorate for Research and Community Service, Ministry of Higher Education, Science, and Technology of the Republic of Indonesia, Institut Teknologi Sepuluh Nopember, under Contract Number 1229/PKS/ITS/2025 for the Fiscal Year 2025.

6-4- Acknowledgments

The authors acknowledge the support provided by the Center for Artificial Intelligence and Digital Technology (KATD) and Institut Teknologi Sepuluh Nopember (ITS), particularly for the computational facilities and technical assistance that facilitated this research.

6-5- Institutional Review Board Statement

Not applicable.

6-6- Informed Consent Statement

Not applicable.

6-7- Conflicts of Interest

The authors declare that there is no conflict of interest regarding the publication of this manuscript. In addition, the ethical issues, including plagiarism, informed consent, misconduct, data fabrication and/or falsification, double publication and/or submission, and redundancies have been completely observed by the authors.

7- References

[1] Zhou, P., Lv, Y., & Wen, W. (2023). The Low-Carbon Transition of Energy Systems: A Bibliometric Review from an Engineering Management Perspective. Engineering, 29, 147–158. doi:10.1016/j.eng.2022.11.010.

[2] Jaiswal, K. K., Chowdhury, C. R., Yadav, D., Verma, R., Dutta, S., Jaiswal, K. S., SangmeshB, & Karuppasamy, K. S. K. (2022). Renewable and sustainable clean energy development and impact on social, economic, and environmental health. Energy Nexus, 7, 100118. doi:10.1016/j.nexus.2022.100118.

[3] Sadeghi, H., Shami, H. O., Moazzami, M., Ahmadi, G., Toghraie, D., Rezaei, M., Dolatshahi, M., & Salahshour, S. (2024). Design an integrated strategic resource planning to analyze the development of renewable energy sources. Energy Strategy Reviews, 53, 101427. doi:10.1016/j.esr.2024.101427.

[4] Cook, D., & Pétursson, J. G. (2025). The role of GIS mapping in multi-criteria decision analysis in informing the location and design of renewable energy projects - A systematic review. Energy Strategy Reviews, 59, 101765. doi:10.1016/j.esr.2025.101765.

[5] Paschetto, A., Caselle, C., & Bonetto, S. M. R. (2025). A GIS-based methodology for hydropower potential assessment: balancing energy production and ecosystem sustainability. Environmental Challenges, 20, 101236. doi:10.1016/j.envc.2025.101236.

[6] Sperring, E., Gaskin, S., & Jordaan, S. M. (2025). Quantifying land-energy interactions of hydropower in the Western United States. Renewable and Sustainable Energy Reviews, 224. doi:10.1016/j.rser.2025.116096.

[7] Tamm, O., & Tamm, T. (2020). Verification of a robust method for sizing and siting the small hydropower run-of-river plant potential by using GIS. Renewable Energy, 155, 153–159. doi:10.1016/j.renene.2020.03.062.

[8] Odiji, C., Adepoju, M., Ibrahim, I., Adedeji, O., Nnaemeka, I., & Aderoju, O. (2021). Small hydropower dam site suitability modelling in upper Benue river watershed, Nigeria. Applied Water Science, 11(8), 136. doi:10.1007/s13201-021-01466-6.

[9] Kucukali, S., Al Bayatı, O., & Maraş, H. H. (2021). Finding the most suitable existing irrigation dams for small hydropower development in Turkey: A GIS-Fuzzy logic tool. Renewable Energy, 172, 633–650. doi:10.1016/j.renene.2021.03.049.

[10] Jafari, M., Fazloula, R., Effati, M., & Jamali, A. (2021). Providing a GIS-based framework for Run-Of-River hydropower site selection: a model based on sustainable development energy approach. Civil Engineering and Environmental Systems, 38(2), 102–126. doi:10.1080/10286608.2021.1893310.

[11] Mochani, M. M., Moridi, A., Tehrani, M. D., Khalili, R., & Haghighi, A. T. (2025). Site Selection and Investment Prioritization for Small Hydropower Plants Using Spatial Multi-Criteria Decision-Making Models. Water Resources Management, 39(13), 6985–7004. doi:10.1007/s11269-025-04279-3.

[12] Akajiaku, U. C., Ohimain, E. I., Olodiama, E. ere B., Eteh, D. R., Winston, A. G., Chukwuemeka, P., Otutu, A. O., Bamiekumo, B. P., & Imoni, O. (2025). Identifying suitable dam sites using geospatial data and machine learning: a case study of the katsina-ala river in Benue State, Nigeria. Earth Science Informatics, 18(3), 497. doi:10.1007/s12145-025-01974-y.

[13] Casali, Y., Aydin, N. Y., & Comes, T. (2022). Machine learning for spatial analyses in urban areas: a scoping review. Sustainable Cities and Society, 85, 104050. doi:10.1016/j.scs.2022.104050.

[14] Hou, Y., Wang, Q., & Tan, T. (2023). Regional suitability assessment for straw-based power generation: A machine learning approach. Energy Strategy Reviews, 49, 101173. doi:10.1016/j.esr.2023.101173.

[15] Rattanarat, J., Jaroensutasinee, K., Jaroensutasinee, M., & Sparrow, E. B. (2025). Driving Mangrove Recovery: Community Engagement and Socio-Economic Shifts in Aquaculture Areas. Emerging Science Journal, 9(5), 2439–2453. doi:10.28991/ESJ-2025-09-05-09.

[16] Hettiarachchi, S., & Bandara, T. R. (2023). Deep Learning-Based Land Cover Classification for Satellite Images of Sri Lanka Using ConvNets. 2023 5th International Conference on Advancements in Computing (ICAC), 585–590. doi:10.1109/ICAC60630.2023.10417674.

[17] Uti, M. N., Md Din, A. H., Yusof, N., & Yaakob, O. (2023). A spatial-temporal clustering for low ocean renewable energy resources using K-means clustering. Renewable Energy, 219, 119549. doi:10.1016/j.renene.2023.119549.

[18] Leng, Z., Chen, L., Liu, F., Yi, B., Liu, Z., Xie, T., & Zhang, Y. (2025). A novel zoning framework for hydro-wind-photovoltaic integrated energy bases based on Laplacian-enhanced clustering and complementarity evaluation. Energy, 341, 139436. doi:10.1016/j.energy.2025.139436.

[19] Luo, W., Johra, H., Borkowski, E., Liu, X., Wen, J., Ouf, M., Capozzoli, A., Nagy, Z., & Kramer, R. (2025). Developing a weighting scheme for building operational performance: A case study from the Netherlands. Building and Environment, 286, 113762. doi:10.1016/j.buildenv.2025.113762.

[20] Hämäläinen, R. P., Lahtinen, T. J., & Virtanen, K. (2024). Generating policy alternatives for decision making: A process model, behavioural issues, and an experiment. EURO Journal on Decision Processes, 12, 100050. doi:10.1016/j.ejdp.2024.100050.

[21] Saharkhiz, M. A., Pradhan, B., Rizeei, H. M., & Jung, H. S. (2020). Land use feature extraction and sprawl development prediction from quickbird satellite imagery using Dempster-Shafer and land transformation model. Korean Journal of Remote Sensing, 36(1), 15–27. doi:10.7780/kjrs.2020.36.1.2.

[22] Fu, X., Wu, X., Zhang, C., Fan, S., & Liu, N. (2022). Planning of distributed renewable energy systems under uncertainty based on statistical machine learning. Protection and Control of Modern Power Systems, 7(1), 1–27. doi:10.1186/s41601-022-00262-x.

[23] Drogkoula, M., Samaras, N., Iatrellis, O., Nathanail, E., & Kokkinos, K. (2025). Systematic review and topic classification of soft computing and machine learning in water resources management. Discover Sustainability, 6(1), 860. doi:10.1007/s43621-025-01832-3.

[24] Hacıoğlu, Ö., Başokur, A. T., Diner, Ç., Meqbel, N., Arslan, H. İ., & Oğuz, K. (2020). The effect of active extensional tectonics on the structural controls and heat transport mechanism in the Menderes Massif geothermal province: Inferred from three-dimensional electrical resistivity structure of the Kurşunlu geothermal field (Gediz Graben, western Anatolia). Geothermics, 85, 101708. doi:10.1016/j.geothermics.2019.07.006.

[25] Xiao, X., Wang, P., Ge, Y., Luo, J., Chen, H., He, Y., Zhang, D., Li, Y., Fang, C., & Lin, H. (2025). GeoKG-HSA: A framework for habitat suitability assessment with geospatial knowledge graphs. International Journal of Applied Earth Observation and Geoinformation, 144, 104921. doi:10.1016/j.jag.2025.104921.

[26] Zachora-Buławska, A., Kędzior, R., & Operacz, A. (2024). Spent geothermal water discharge to rivers: Risk or environmental benefit? Science of the Total Environment, 954, 176527. doi:10.1016/j.scitotenv.2024.176527.

[27] Gizaw, E. A., Bawoke, G. T., Alemu, M. M., & Anteneh, Z. L. (2023). Spatial analysis of groundwater potential using remote sensing and GIS-based multi-criteria decision analysis method in Fetam-Yisir catchment, Blue Nile Basin, Ethiopia. Applied Geomatics, 15(3), 659–681. doi:10.1007/s12518-023-00518-7.

[28] Zhu, Z., Qiu, S., & Ye, S. (2022). Remote sensing of land change: A multifaceted perspective. Remote Sensing of Environment, 282, 113266. doi:10.1016/j.rse.2022.113266.

[29] Utama, W., & Indriani, R. F. (2021). Regional Physiographic Study for the Hydrology of Kali Lamong Watershed Area. IOP Conference Series: Earth and Environmental Science, 936(1), 012032. doi:10.1088/1755-1315/936/1/012032.

[30] Chelariu, O. E., Minea, I., & Iațu, C. (2023). Geo-hazards assessment and land suitability estimation for spatial planning using multi-criteria analysis. Heliyon, 9(7), 18159. doi:10.1016/j.heliyon.2023.e18159.

[31] Areri, D. C., & Bibi, T. S. (2023). Identification of small-scale hydropower potential sites using geographic information system and hydrologic modeling technique: Awata river, Genale Dawa basin, Ethiopia. Energy Reports, 9, 2405–2419. doi:10.1016/j.egyr.2023.01.081.

[32] Fasipe, O. A., Izinyon, O. C., & Ehiorobo, J. O. (2021). Hydropower potential assessment using spatial technology and hydrological modelling in Nigeria river basin. Renewable Energy, 178, 960–976. doi:10.1016/j.renene.2021.06.133.

[33] Rayat, S. S., Thapa, S., Basnet, R., Sharma, V., Rathod, A. P. S., & Kukreti, K. (2025). A Novel Approach for Adaptive Spatial Suitability Index with Hybrid ML-DL for Renewable Energy Site Selection. 2025 IEEE 7th International Conference on Computing, Communication and Automation (ICCCA), 1–6. doi:10.1109/iccca66364.2025.11325167.

[34] Ouchani, F. zahra, Jbaihi, O., Alami Merrouni, A., Ghennioui, A., & Maaroufi, M. (2022). Geographic Information System-based Multi-Criteria Decision-Making analysis for assessing prospective locations of Pumped Hydro Energy Storage plants in Morocco: Towards efficient management of variable renewables. Journal of Energy Storage, 55, 105751. doi:10.1016/j.est.2022.105751.

[35] Patel, D., Darji, K.R., Dubey, A.K., Gupta, P., Singh, R.P. (2024). Application of Open-Source Geospatial and Modeling Techniques for Flood Assessment and Management—A Case of Flood 2017, Rel River Catchment. Innovation in Smart and Sustainable Infrastructure, ISSI 2022. Lecture Notes in Civil Engineering, Springer, Singapore. doi:10.1007/978-981-99-3557-4_5.

[36] Özkurt, C., Canay, Ö., Tunç, E. A., Aydin, E., & Velioğlu, B. S. (2025). Renewable Energy Source Ranking and Analysis Using Fuzzy MCDM, ML, and XAI Techniques. Baltic Journal of Modern Computing, 13(3), 656–679. doi:10.22364/bjmc.2025.13.3.06.

[37] Mitjana, F., Denault, M., & Demeester, K. (2022). Managing chance-constrained hydropower with reinforcement learning and backoffs. Advances in Water Resources, 169, 104308. doi:10.1016/j.advwatres.2022.104308.

[38] Sahin, M. E., & Ozbay Karakus, M. (2024). Smart hydropower management: utilizing machine learning and deep learning method to enhance dam's energy generation efficiency. Neural Computing and Applications, 36(19), 11195–11211. doi:10.1007/s00521-024-09613-1.

[39] López-Bravo, C., Mora-López, L., Sidrach-deCardona, M., & Márquez-Ballesteros, M. J. (2024). A comprehensive analysis based on GIS-AHP to minimise the social and environmental impact of the installation of large-scale photovoltaic plants in south Spain. Renewable Energy, 226. doi:10.1016/j.renene.2024.120387.

[40] Öztürk, M. Z., Poyraz, M., Duman, H., & Taşoğlu, E. (2025). A geospatial approach to understanding sinkhole formation in Akgöl Wetland, Türkiye. Environmental Earth Sciences, 84(8), 209. doi:10.1007/s12665-025-12225-0.

[41] Kobayashi, T., Matsuo, K., Ando, R., Nakano, T., & Watanuki, G. (2025). High-resolution image on terminus of fault rupture: relationship with volcanic hydrothermal structure. Geophysical Journal International, 240(2), 1196–1214. doi:10.1093/gji/ggae435.

[42] Kabeyi, M. J. B., & Olanrewaju, O. A. (2025). Social Value of Energy Sources for Decentralized Generation. 2025 13th International Conference on Smart Grid (icSmartGrid), 1–8. doi:10.1109/ICSMARTGRID66138.2025.11071840.

[43] Indriani, R. F., & Utama, W. (2023). Physiographic Study for Hydrology of Benowo Region Surabaya. IOP Conference Series: Earth and Environmental Science, 1127(1), 012019. doi:10.1088/1755-1315/1127/1/012019.

[44] Indriani, R. F., Anjasmara, I. M., Utama, W., Paramita, E. G. K., & Nainggolan, R. A. O. (2023). Comparative Analysis of Physiograpic Study for Hydrology of Benowo Region, Surabaya. IOP Conference Series: Earth and Environmental Science, 1250(1), 12015. doi:10.1088/1755-1315/1250/1/012015.

[45] Darji, K. R., Vyas, U. H., Patel, D., & Dewals, B. (2024). A Dam Break Analysis of Damanganga Dam Using HEC-RAS 2D Hydrodynamic Modelling and Geospatial Techniques. Innovation in Smart and Sustainable Infrastructure, ISSI 2022. Lecture Notes in Civil Engineering, Springer, Singapore. doi:10.1007/978-981-99-3557-4_1.

[46] Dibs, H., Ali, A. H., Al-Ansari, N., & Abed, S. A. (2023). Fusion Landsat-8 Thermal TIRS and OLI Datasets for Superior Monitoring and Change Detection using Remote Sensing. Emerging Science Journal, 7(2), 428–444. doi:10.28991/ESJ-2023-07-02-09.

[47] Sun, T., Yan, N., Zhu, W., & Zhuang, Q. (2024). Assessing a machine learning-based downscaling framework for obtaining 1km daily precipitation from GPM data. Heliyon, 10(17), 36368. doi:10.1016/j.heliyon.2024.e36368.

[48] Galang, E. I. N. E., Bennett, E. M., Hickey, G. M., Baird, J., Harvey, B., & Sherren, K. (2025). Participatory scenario planning: A social learning approach to build systems thinking and trust for sustainable environmental governance. Environmental Science and Policy, 164, 103997. doi:10.1016/j.envsci.2025.103997.

[49] Eshra, N. M., Zobaa, A. F., & Abdel Aleem, S. H. E. (2021). Assessment of mini and micro hydropower potential in Egypt: Multi-criteria analysis. Energy Reports, 7, 81–94. doi:10.1016/j.egyr.2020.11.165.

[50] Almeida, R. M., Schmitt, R. J., Castelletti, A., Flecker, A. S., Harou, J. J., Heilpern, S. A., Kittner, N., Mathias Kondolf, G., Opperman, J. J., Shi, Q., Gomes, C. P., & McIntyre, P. B. (2022). Strategic planning of hydropower development: balancing benefits and socioenvironmental costs. Current Opinion in Environmental Sustainability, 56, 101175. doi:10.1016/j.cosust.2022.101175.

[51] Adem, M., Davíðsdóttir, B., & Arnalds, S. S. (2021). Preparation of the abaya project for geothermal sustainability assessment protocol in Ethiopia. 2021 Geothermal Rising Conference: Using the Earth to Save the Earth, GRC 2021, 3-6 October, 2021, Diego, United States.

[52] Ren, Q., Handler, R., Shonnard, D., & You, Z. (2025). Assessment of Sustainability of Locomotive Propulsion Technologies. International Conference on Transportation and Development 2025, 853–865. doi:10.1061/9780784486207.074.

[53] Doğan, A. (2026). An ensemble unsupervised machine learning–GIS framework for transparent and data-driven offshore wind farm siting. Ocean Engineering, 344, 123703. doi:10.1016/j.oceaneng.2025.123703.

[54] Hung, F., & Yang, Y. C. E. (2021). Assessing Adaptive Irrigation Impacts on Water Scarcity in Nonstationary Environments—A Multi-Agent Reinforcement Learning Approach. Water Resources Research, 57(9), 2020 029262,. doi:10.1029/2020WR029262.

[55] Lu, Y., & Ben-Zion, Y. (2022). Validation of seismic velocity models in southern California with full-waveform simulations. Geophysical Journal International, 229(2), 1232–1254. doi:10.1093/gji/ggab534.

[56] Punys, P., Jurevičius, L., & Balčiūnas, A. (2024). HYPOSO Map Viewer: A Web-Based Atlas of Small-Scale Hydropower for Selected African and Latin American Countries. Water (Switzerland), 16(9), 1276. doi:10.3390/w16091276.

[57] Catalano, G. A., Maci, F., Valenti, F., D'Urso, P. R., & Arcidiacono, C. (2023). Assessing Application Potential of Species Distribution Models to the Case Study of Citrus in Eastern Sicily. AIIA 2022: Biosystems Engineering Towards the Green Deal, AIIA 2022, Lecture Notes in Civil Engineering, Springer, Cham, Switzerland. doi:10.1007/978-3-031-30329-6_114.

[58] Stratoulias, D., Nuthammachot, N., Dejchanchaiwong, R., Tekasakul, P., & Carmichael, G. R. (2024). Recent Developments in Satellite Remote Sensing for Air Pollution Surveillance in Support of Sustainable Development Goals. Remote Sensing, 16(16), 2932. doi:10.3390/rs16162932.

[59] Wadoux, A. M. J. C., Heuvelink, G. B. M., de Bruin, S., & Brus, D. J. (2021). Spatial cross-validation is not the right way to evaluate map accuracy. Ecological Modelling, 457, 109692. doi:10.1016/j.ecolmodel.2021.109692.

[60] Naikoo, M. W., Shahfahad, Talukdar, S., Rihan, M., Ahmed, I. A., Thi Hang, H., Ishtiaq, M., & Rahman, A. (2024). A Geospatial Approach to Mapping and Monitoring Real Estate-Induced Urban Expansion in the National Capital Region of Delhi. PFG – Journal of Photogrammetry, Remote Sensing and Geoinformation Science, 92(2), 177–200. doi:10.1007/s41064-024-00278-y.

[61] Goyal, H., Joshi, N., & Sharma, C. (2018). An Empirical Analysis of Geospatial Classification for Agriculture Monitoring. Procedia Computer Science, 132, 1102–1112. doi:10.1016/j.procs.2018.05.025.

[62] Zhao, G., Ping, J., Mei, X., Leng, W., Deng, Q., & Fan, X. (2025). Prediction of regional hydrothermal geothermal resource carrying capacity based on multi-level fuzzy comprehensive evaluation: A case study of Zhengzhou, China. Case Studies in Thermal Engineering, 75, 107156. doi:10.1016/j.csite.2025.107156.

[63] Steward, R., Chopin, P., & Verburg, P. H. (2024). Supporting spatial planning with a novel method based on participatory Bayesian networks: An application in Curaçao. Environmental Science and Policy, 156, 103733. doi:10.1016/j.envsci.2024.103733.

[64] Mishra, A. K., Upadhyay, A., Mishra, P. K., Srivastava, A., & Rai, S. C. (2023). Evaluating geo-hydrological environs through morphometric aspects using geospatial techniques: A case study of Kashang Khad watershed in the Middle Himalayas, India. Quaternary Science Advances, 11. doi:10.1016/j.qsa.2023.100096.

[65] Dibaba, W. T., Dibaba, B. T., & Hirpa, G. D. (2025). Spatiotemporal analysis of the wetland dynamics using geospatial techniques: case of Gojeb River sub-basin, Ethiopia. Environmental Monitoring and Assessment, 197(8), 844. doi:10.1007/s10661-025-14276-z.

[66] Kassem, M. A., Moscariello, A., & Hollmuller, P. (2025). Navigating risk in geothermal energy projects: A systematic literature review. Energy Reports, 13, 696–712. doi:10.1016/j.egyr.2024.12.052.

[67] Wang, L., Yu, Z., Zhang, Y., & Yao, P. (2023). Review of machine learning methods applied to enhanced geothermal systems. Environmental Earth Sciences, 82(3), 1–19. doi:10.1007/s12665-023-10749-x.

[68] Carella, E., Orusa, T., Viani, A., Meloni, D., Borgogno- mondino, E., & Orusa, R. (2022). An Integrated, Tentative Remote-Sensing Approach Based on NDVI Entropy to Model Canine Distemper Virus in Wildlife and to Prompt Science-Based Management Policies. Animals, 12(8), 108049. doi:10.3390/ani12081049.

[69] Khamit, N., Jangulova, G., Kakimzhanov, Y., Kyrgyzbay, K., Zhumatayev, S., Atalykova, N., & Kozhaev, Z. (2025). Geodynamic Processes Monitoring of Subway Infrastructure Using Geodetic and Remote Sensing Methods. Civil Engineering Journal, 11(10), 4353–4379. doi:10.28991/CEJ-2025-011-10-021.

[70] Bai, J., Ren, J., Yang, Y., Xiao, Z., Yu, W., Havyarimana, V., & Jiao, L. (2022). Object Detection in Large-Scale Remote-Sensing Images Based on Time-Frequency Analysis and Feature Optimization. IEEE Transactions on Geoscience and Remote Sensing, 60. doi:10.1109/TGRS.2021.3119344.

[71] Sarkar, A., Lanier, M., Alfeld, S., Feng, J., Garnett, R., Jacobs, N., & Vorobeychik, Y. (2024). A Visual Active Search Framework for Geospatial Exploration. 2024 IEEE/CVF Winter Conference on Applications of Computer Vision (WACV), 8301–8310. doi:10.1109/WACV57701.2024.00813.

[72] Basumatary, S., & Maji, S. (2025). Applications for Water Resources Management in Foot-Hill: A Comprehensive Review. Soft Computing and Geospatial Techniques in Water Resources Engineering, HYDRO 2023, Lecture Notes in Civil Engineering, Springer, Singapore. doi:10.1007/978-981-97-7467-8_38.

[73] Chao, J., Zhao, Z., Lai, Z., Liu, J., Hu, Y., & Cui, D. (2025). Exploring geothermal potential with robust satellite techniques using MODIS LST data. Geothermics, 132, 103414. doi:10.1016/j.geothermics.2025.103414.

[74] He, Q., Liu, J. L., Eschapasse, L., Beveridge, E. H., & Brown, T. I. (2022). A comparison of reinforcement learning models of human spatial navigation. Scientific Reports, 12(1), 13923. doi:10.1038/s41598-022-18245-1.

[75] Ahn, J. M., Jeong, W., Lee, H., & Kim, K. (2025). Hyperspectral imaging-based land use classification using a hybrid Convolutional Neural network-vision transformer model. Environmental Technology and Innovation, 39, 104317. doi:10.1016/j.eti.2025.104317.

[76] Tubiello, F. N., Conchedda, G., Casse, L., Hao, P., De Santis, G., & Chen, Z. (2023). A new cropland area database by country circa 2020. Earth System Science Data, 15(11), 4997–5015. doi:10.5194/essd-15-4997-2023.

[77] Shoedarto, R. M., Tada, Y., Kashiwaya, K., Koike, K., & Iskandar, I. (2022). Advanced characterization of hydrothermal flows within recharge and discharge areas using rare earth elements, proved through a case study of two-phase reservoir geothermal field, in Southern Bandung, West Java, Indonesia. Geothermics, 105(April), 102507. doi:10.1016/j.geothermics.2022.102507.

[78] Bui, Q. D., Luu, C., Ha, H., Do, V. C., & Tran, T. X. (2025). Surface water salinity modeling for the Mekong Delta of Vietnam using hourly salinity observed data, remote sensing, and machine learning models. Advances in Space Research, 76(3), 1417–1437. doi:10.1016/j.asr.2025.05.055.

[79] Rau, K., Eggensperger, K., Schneider, F., Blaschek, M., Hennig, P., & Scholten, T. (2025). Quantifying spatial uncertainty to improve soil predictions in data-sparse regions. Soil, 11(2), 833–847. doi:10.5194/soil-11-833-2025.

[80] Shanthala Devi, B. S., Murthy, M. S. R., Debnath, B., & Jha, C. S. (2013). Forest patch connectivity diagnostics and prioritization using graph theory. Ecological Modelling, 251, 279–287. doi:10.1016/j.ecolmodel.2012.12.022.

[81] Shen, Y., Ren, Z., Fan, J., Xiao, J., Zhang, Y., & Liu, X. (2025). Fine-Scale Risk Mapping for Dengue Vector Using Spatial Downscaling in Intra-Urban Areas of Guangzhou, China. Insects , 16(7), 661. doi:10.3390/insects16070661.

[82] Awasthi, A., & Rishi, M. S. (2025). Assessing groundwater potential for sustainable development in the transboundary aquifers of River Ravi, India: an integrated geospatial and AHP approach. Environmental Earth Sciences, 84(14), 419. doi:10.1007/s12665-025-12415-w.

[83] Asghar, A., Su, L.-j., Zhao, B., & Usmani, N. A. (2023). Integrating predictive modeling techniques with geospatial data for landslide susceptibility assessment in northern Pakistan. Journal of Mountain Science, 20(9), 2603–2627. doi:10.1007/s11629-023-8029-2.

[84] Yan, A. (2025). AI-powered framework for rural landscape design: high-resolution geospatial analysis, multi-objective optimization, and real-time visualization. Second International Conference on Intelligent Transportation and Smart Cities (ICITSC 2025), 69. doi:10.1117/12.3073796.

[85] Solbrekke, I. M., & Sorteberg, A. (2024). Norwegian offshore wind power—Spatial planning using multi-criteria decision analysis. Wind Energy, 27(1), 5–32. doi:10.1002/we.2871.

[86] Ni, S., & Al-qaness, M. A. A. (2026). PTCVS-net: Patch-based transformer-CNN with variable sparse attention network for sEMG-based gesture recognition. Applied Soft Computing, 187, 114316. doi:10.1016/j.asoc.2025.114316.

[87] Bhattarai, U., Maraseni, T., Apan, A., & Devkota, L. P. (2023). Rationalizing donations and subsidies: Energy ecosystem development for sustainable renewable energy transition in Nepal. Energy Policy, 177, 177. doi:10.1016/j.enpol.2023.113570.

[88] Coverdale, T. C., Boucher, P. B., Singh, J., & Davies, A. B. (2025). Quantifying aboveground herbaceous biomass in grassy ecosystems: a comparison of field and high-resolution UAV-LiDAR approaches. Remote Sensing in Ecology and Conservation. doi:10.1002/rse2.70023.

[89] Dosis, S., Petropoulos, G. P., & Kalogeropoulos, K. (2023). A Geospatial Approach to Identify and Evaluate Ecological Restoration Sites in Post-Fire Landscapes. Land, 12(12), 12122183. doi:10.3390/land12122183.

[90] Tende, A. W., Miner Iiiya, M., Habu, S., Gajere, J. N., Iyakwari, S., & Aminu, M. D. (2025). GIS-based multi-criteria predictive modelling for geothermal energy exploration. Energy Geoscience, 6(2), 100409. doi:10.1016/j.engeos.2025.100409.

[91] Mngadi, M., Odindi, J., Mutanga, O., & Sibanda, M. (2022). Quantitative remote sensing of forest ecosystem services in sub-Saharan Africa's urban landscapes: a review. Environmental Monitoring and Assessment, 194(4), 242. doi:10.1007/s10661-022-09904-x.

[92] Gkeka-Serpetsidaki, P., & Tsoutsos, T. (2023). Integration criteria of offshore wind farms in the landscape: Viewpoints of local inhabitants. Journal of Cleaner Production, 417. doi:10.1016/j.jclepro.2023.137899.